INTERNATIONAL JOURNAL OF CLIMATOLOGY
*Int. J. Climatol.* **34**: 780–792 (2014)
Published online 20 May 2013 in Wiley Online Library
(wileyonlinelibrary.com) DOI: 10.1002/joc.3724

RMetS
Royal Meteorological Society

# A synoptic climatology of the near-surface wind along the west coast of South America

David A. Rahn[a,b,*] and René D. Garreaud[a,c]

[a] *Departamento de Geofísica, Facultad de Ciencias Físicas y Matemáticas, Universidad de Chile, Santiago, Chile*
[b] *Atmospheric Science Program, Department of Geography, University of Kansas, Lawrence, Kansas*
[c] *Center for Climate and Resilience Research (CR)2, Universidad de Chile*

**ABSTRACT:** Prevailing wind along the west coast of South America is equatorward, driven by the southeast Pacific anticyclone. The wind induces strong coastal upwelling that supports one of the most important fisheries in the world. This region lacks a dense network of *in situ* observations, so the high resolution (0.313°) NCEP Climate Forecast System Reanalysis is used here to present a synoptic climatology of the coastal wind along the Chile/Peru coast. Covariability between the alongshore pressure gradient and alongshore wind, which was previously identified for synoptic time scales near central Chile, is generalized for the whole coast and over annual time scales. Particular attention is paid to three prominent upwelling regions: Pisco (14.8°S), Punta Lengua de Vaca (30.0°S), and Punta Lavapie (36.4°S). Previous work has identified local maxima at these points but these are embedded in a broader low-level jet that exhibits a marked seasonal cycle of strong wind days due to the migration of the anticyclone and is associated with a shift of both the mean wind and a more frequent recurrence of strong wind events. Alongshore wind near Pisco is normally distributed year-round with a seasonal shift in the mean. Larger variability in the mean and distribution is found at Lavapie, associated with the seasonal change in storm tracks. The synoptic evolution that drives high-wind events at each location is characterized. A midlevel trough and surface cyclone precede wind maxima at each location and are followed by strong midlevel ridging and a strengthened surface anticyclone.

KEY WORDS coastal wind; eastern boundary upwelling system; South America; synoptic climatology

*Received 4 July 2012; Revised 5 February 2013; Accepted 19 April 2013*

## 1. Introduction

Offshore of Peru-Chile there is a major eastern boundary upwelling system that accounts for 16–20% (12 million tonnes) of the global fish catch (Sherman and Hempel, 2009). Large-scale tropospheric subsidence maintains the southeast Pacific (SEP) subtropical anticyclone, which forces equatorward wind along most of the west coast of South America. Low-level alongshore flow fosters ocean upwelling through Ekman transport and Ekman pumping near the shore, maintaining a coastal band of cold waters that extends from about 40°S to the equator (Hill *et al.*, 1998; Aguirre *et al.*, 2012). Ocean eddies transport coastal waters westward extending the sea surface temperature cold anomalies well offshore (Capet *et al.*, 2008). Both the relatively cold sea surface and a persistent deck of low-level clouds contribute to the diabatic cooling of the lower troposphere over the SEP, which at subtropical latitudes tends to be compensated by enhanced subsidence, closing the loop between atmospheric and oceanic processes (Wang *et al.*, 2005).

Direct and indirect evidence reveals substantial alongshore variability of the coastal wind, including three prominent low-level wind speed maxima near Pisco (14.8°S 76.6°W), Punta Lengua de Vaca (LdV, 30.0°S 72.2°W), and Punta Lavapie (36.4°S 73.8°W). Upwelling is particularly intense in these three areas of wind maxima, and they have received attention due to their impact on the local ocean circulation that motivated several dedicated field campaigns such as CUEA JOINT-II (Brink *et al.*, 1978) and VOCALS-Rex Peru Cruise (Grados *et al.*, 2010) near Pisco, VOCALS-CUpEx at LdV (Garreaud *et al.*, 2011), and CUpEx II at Lavapie (Montecinos *et al.*, 2011).

While previous studies have provided a broad description of the wind field over the SEP (Halpern *et al.* 2002) as well as some detailed information on specific areas of wind maxima, an integrated description of the near-surface wind along the west coast of South America is hampered by the lack of observations. Radiosondes are routinely launched from only three coastal sites spanning over 2400 km: Lima (12°S), Antofagasta (23°S), and Santo Domingo (33°S). The Chilean and Peruvian weather services also maintain about a dozen surface stations at coastal sites complemented by a similar number of stations operated by other institutions. Nevertheless, most of these stations are a few kilometres

* Correspondence to: David A. Rahn, Atmospheric Science Program, Department of Geography, University of Kansas, 1475 Jayhawk Blvd., 201 Lindley Hall, Lawrence, KS 66045–7613. E-mail: darahn@ku.edu

inland and/or sheltered from the coastal wind, so their use for describing the alongshore flow is questionable (R. Muñoz 2012, personal communication). The region also lacks systematic, long-term monitoring of the near shore wind by coastal buoys or high frequency (HF) radars, and ship-borne observations ingested in Comprehensive Ocean-Atmosphere Data Set (COADS) (Woodruff *et al.*, 2011) are restricted around major ports.

Other studies have relied on satellite-borne scatterometer data (Halpern *et al.* 2002; Garreaud and Muñoz, 2005; Muñoz, 2008) or atmospheric reanalysis. Satellite scatterometer measurements, however, contain a 25-km wide blind spot along the coast and have at most two passes over one area per day. Reanalysis projects assimilate surface, upper-air, and satellite data into a short-term numerical forecast, thus providing the best approximation of the three-dimensional atmospheric state several times daily and have been available for several decades now. Older atmospheric reanalysis such as the NCEP/NCAR (Kalnay *et al.*, 1996) have a 2.5° (∼250 km) horizontal grid spacing and only three vertical levels below 2 km, which miss relevant details of mesoscale phenomena such as local wind maxima tied to coastal topography. More recent work uses better datasets such as the ERA-Interim reanalysis (Dee *et al.*, 2011), which is ∼80 km and 60 vertical levels with a top at 0.1 hPa.

In this work we take advantage of the recently released Climate Forecast System Reanalysis (CFSR, Saha *et al.*, 2010) to provide a large-scale, long-term description of the near-surface coastal winds off western South America as well as dynamical analysis focused on the synoptic-scale environment that characterize strong wind events in selected areas where they are recurrent. The CFSR has 64 vertical levels and is available at a horizontal resolution of 0.313° (comparable with QuikSCAT), which is a considerable improvement over previous reanalyses, with a reanalysis field every 6 h and model forecasts every hour since 1979. The better resolution of the CFSR data provides more detail of the near-coast 10-m wind and is validated against QuikSCAT data. The CFSR resolution, however, is not enough to describe very localized wind maxima (the so-called coastal jets) near major capes along the coast. In Section 2 we present the regular cycles of the large-scale wind field (seasonal and diurnal) as well as a discussion on the relationship between the coastal jet and the broader low-level jets. Section 3 describes how changes in the frequency distribution of daily winds lead to the observed intraseasonal variability of the wind field, with emphasis on the three regions of strong winds (near Pisco, LdV, and Lavapie). Here we also describe the interannual variability of the coastal winds. Section 4 addresses the structural evolution and synoptic forcing of particularly strong wind events in the areas of wind maxima. A summary of our main findings is presented in Section 5.

## 2. The mean annual and diurnal cycles

### 2.1. Large-scale context

Before a detailed analysis of the mean coastal wind off South America, it is instructive to describe the climatological annual cycle of sea level pressure (SLP) and near-surface wind in a broader context. To this effect, Figure 1(a) shows the austral summer (DJF) and winter (JJA) long-term mean SLP from the CFSR. For this and all other plots, the 00 UTC time is used mainly because this is close to when the maximum diurnal wind speed takes place. Local standard time in Chile is UTC-4. Throughout the year, the mean centre of the SEP anticyclone experiences minor changes in its longitudinal position (100–90°W) and intensity (1021–1024 hPa), being slightly more intense in spring. The anticyclone reaches its southernmost position during summer with its centre at ∼35°S, retracting northward during fall and winter when its centre is located at ∼27°S. The poleward

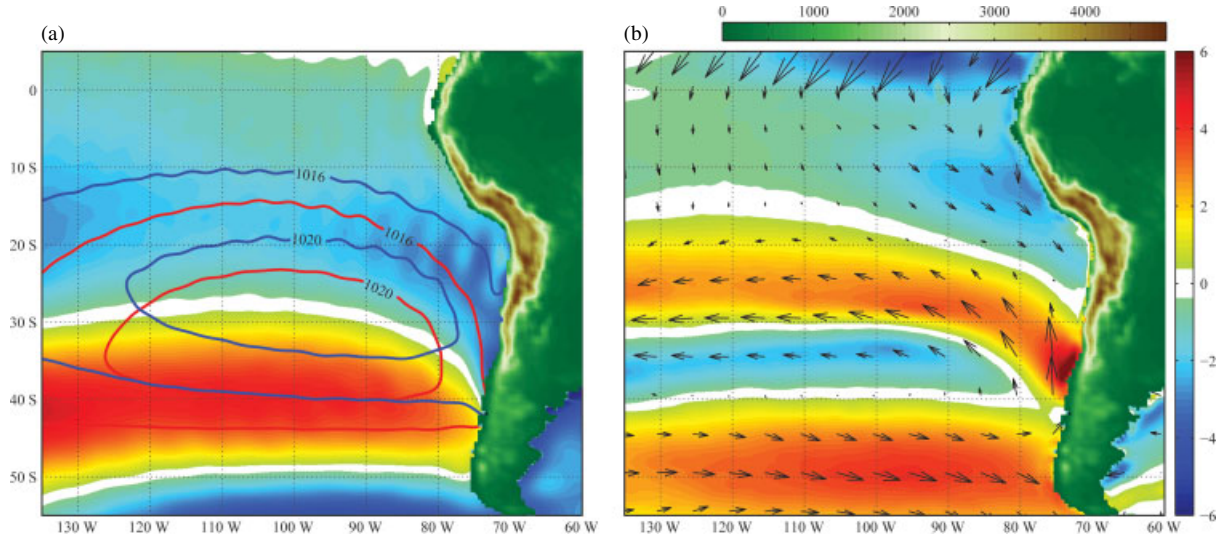


Figure 1. (a) Mean SLP (hPa) for DJF (red contours) and JJA (blue contours) and DJF-JJA (colour). (b) DJF-JJA 10-m wind speed difference ($m\,s^{-1}$, colour) and vector difference. Data from CFSR at 00 UTC. Vectors shown at every 10th grid point.

 

migration of the anticyclone during summer is part of a basin-wide increase in SLP in a band along 40°S and is consistent with large-scale changes in the position of the intertropical convergence zone and the development of the South American monsoon (Rodwell and Hoskins, 2001). Elsewhere over the SEP, the summer SLP values are lower than their winter counterparts. Of special interest is the large winter-to-summer troughing along the coast of north-central Chile (20–35°S). Over the continent the largest winter-to-summer surface pressure drop occurs precisely at subtropical latitudes (masked in Figure 1(a)), leading to the formation of a continental low (Seluchi *et al.*, 2003).

The summer minus winter surface wind difference is displayed in Figure 1(b) along with the seasonal difference in wind speed. Over the open ocean, the westerly wind weakens from winter to summer at subtropical latitudes (25–35°S) and strengthens at midlatitudes (45–55°S), just as expected from the seasonal displacement of the SEP anticyclone. Interestingly, the area of the largest winter-to-summer decrease in surface wind speed is collocated with the largest increase in SLP, indicative of the summertime suppression of transient wind events. Along the South American west coast, there is a dipole of the seasonal wind speed difference with a summer increase at subtropical latitudes (off central Chile) and a decrease at lower latitudes (off Ecuador, Perú, and northern Chile). Both the annual mean and difference in wind vectors are nearly parallel to the coastline, indicative that the seasonal changes in wind speed are largely produced by changes in the alongshore wind component.

### 2.2. Coastal conditions

We now describe the annual cycle of the coastal wind, illustrated in Figure 2 by the long-term bi-monthly means of the 00 UTC wind from 32 years of CFSR data (1979–2010, upper panel) and 11 years of QuikSCAT measurements (1999–2009, lower panel). Both climatologies agree in the overall structure and seasonal cycle (correlations >0.8 for the wind speed field near the coast), but CFSR wind speeds tend to be higher than QuikSCAT values near the coast. The overestimation is larger in the high-wind areas along coast where the

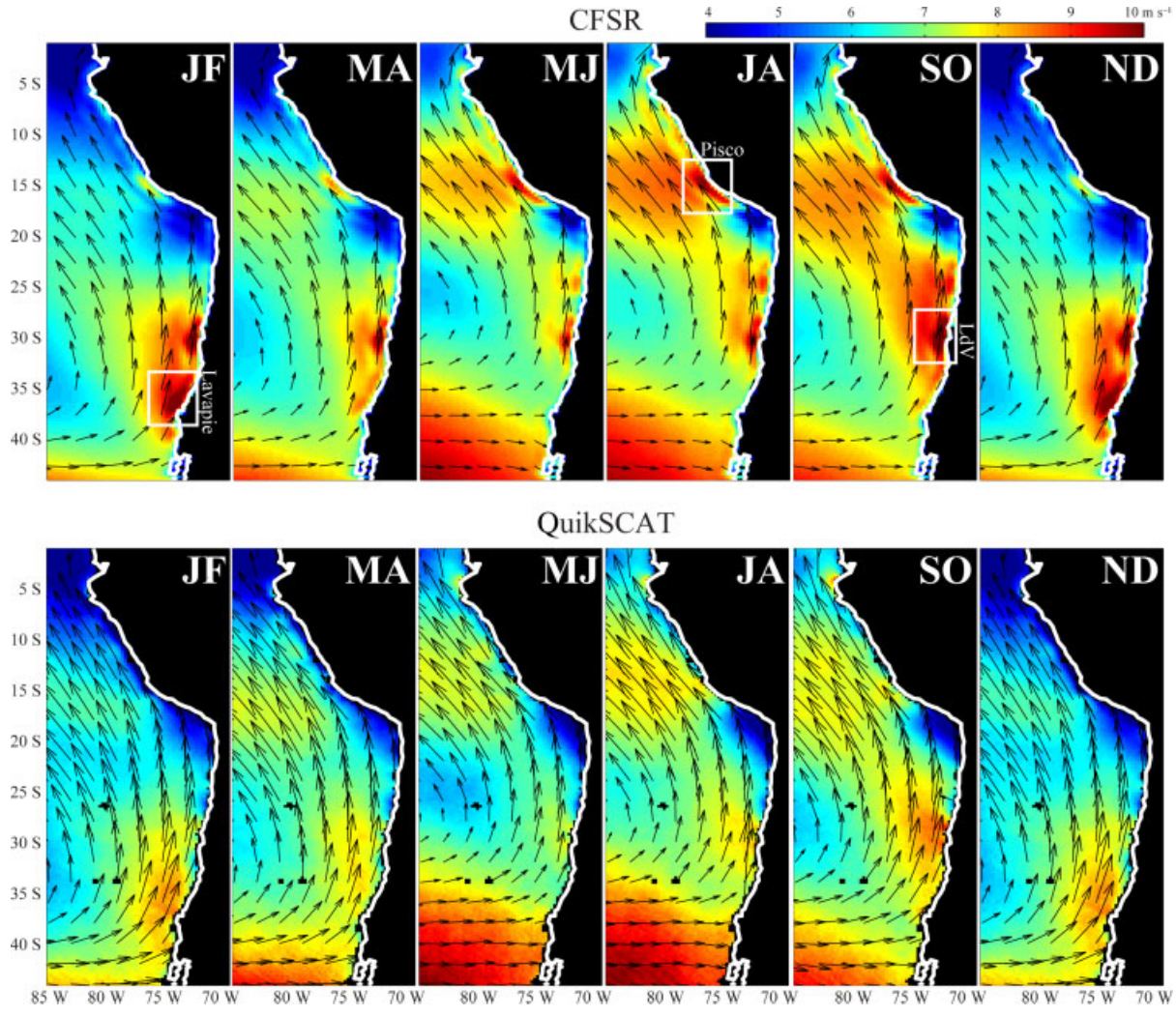


Figure 2. Bimonthly mean of the 10-m wind speed ($m\,s^{-1}$) from (top) the CFSR at 00 UTC (1979–2010) and (bottom) the afternoon satellite pass (~23 UTC) of QuikSCAT (1999–2009). Vectors shown at every eight grid point.

 

CFSR bias is about $1\,m\,s^{-1}$. Some assimilation artefacts in the CFSR near the coast are also evident, presumably because of the Gibb's effect in spectral models that occurs near sharply rising terrain (Lindberg and Broccoli, 1996). The Gibb's effect appears as alternating, banded magnitudes with their long axes oriented in the same direction as the topography (Andes), which is the source of this error. Despite these problems, CFSR does capture the fine-scale alongshore wind variations, evident in QuikSCAT as well. The high-resolution maps in Figure 2 also confirm the year-round dominance of the alongshore wind component at low and subtropical latitudes in the near coastal region with the notable exception of the sector just north of the Arica bight (16–18°S, where the coastline turns abruptly) where the southerly wind impinges on the coast obliquely.

During austral summer (ND–JF) there is a broad region of high-wind speed extending off central Chile and lower wind speed farther north. Both CFSR and QuikSCAT exhibit a local maximum of southerly wind (nearly alongshore) just north of Lavapie. A secondary maximum near LdV is present in CFSR, but only hinted at in QuikSCAT. From March to June the alongshore wind decreases off central Chile and westerly wind becomes dominant in the coastal zone south of 35°S. At the same time, southeasterly wind increases in a broad area at lower latitudes, reaching a maximum in austral winter (JA) off the Pisco region in central Perú. The Pisco maximum is still present in early spring (SO) but it has a rapid demise in November, in agreement with DeWitte *et al.* (2011). During spring the largest wind speed is found off LdV, associated with the strong southerly wind that fosters intense coastal upwelling in this region. The CFSR data also suggests a late-winter/early-spring maximum off Mejillones (23°S), which is another region of enhanced upwelling (Escribano *et al.*, 2004). However, observations of the wind here are limited and such a feature is much weaker in QuikSCAT.

Seasonal changes of the wind along the west coast of South America must be related to changes in the mean seasonal forcing, which is likely associated with the alongshore pressure gradient (APG) based on the findings of Garreaud and Muñoz, 2005 and Muñoz and Garreaud (2005) for synoptic time scales. The APG is depicted in Figure 3 and was calculated at each grid point along the coast as $\Delta SLP/\Delta d$, where $\Delta SLP$ is the difference between the SLP one grid point northward and one grid point southward along the coast and $\Delta d$ (typically ~70 km) is the straight-line distance between the grid point northward and southward. The strongest wind in central and southern Chile (off LdV and Lavapie) coincides with the greatest APG, while the light wind in the Arica Bight is associated with an APG near zero. Large seasonal variations in the APG are evident near Lavapie. During the summer when the alongshore wind is strong, the APG is the greatest along the entire central coast of Chile, but during JJA when the alongshore wind is weak, the mean APG actually becomes negative near Lavapie. The APG near LdV is more consistent throughout the year, but it too has a seasonal dependence and is strongest during the spring (SON) upwelling season. Another local maximum in the APG is at Pisco (albeit weaker and with less seasonal variations than their Chilean counterparts) is greatest during JJA. The seasonal covariability between the alongshore wind and the pressure gradient along the western coast of South America expands an early result in Muñoz and Garreaud (2005) that reported the same association for central Chile at synoptic scales (cf. Figure 13 in Muñoz and Garreaud, 2005). We will re-examine this association at different latitudes in Section 4.

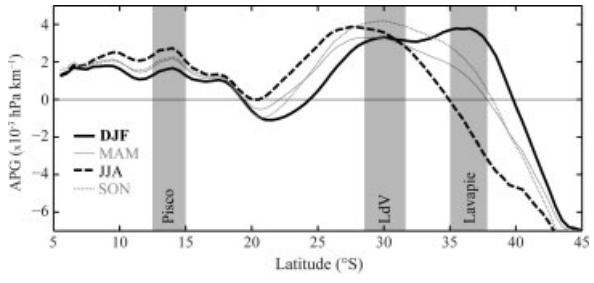


Figure 3. The APG ($10^{-3}$ hPa $km^{-1}$) from CFSR at 00 UTC calculated as described in the text for each season, which is indicated in the lower left. The major upwelling locations are indicated by the grey regions.

### 2.3. Diurnal cycle

Another relevant climatological feature is the mean diurnal cycle of the surface wind. Using QuikSCAT data supplemented with a month-long numerical simulation, Muñoz (2008) analysed this regular cycle over the subtropical SE Pacific (17–40°S) concluding that the afternoon minus morning wind differences are largest along the coast between 20–30°S and mostly meridional (not the classical sea-breeze). Following this approach, Figure 4 shows the bi-monthly averages of 00 minus 12 UTC (evening minus morning) wind vectors and wind speed from CFSR. In line with Muñoz (2008), the largest diurnal cycle is found off north-central Chile (including the LdV region) in spring and summer during the high-wind season there. The diurnal difference in north-central Chile is largely caused by the daytime increase in the southerly, coast-parallel flow. Farther south around Lavapie, wind speed also increases in the afternoon during summer, but a greater part of the diurnal cycle is due to enhanced onshore flow. In contrast, the diurnal variation along the south-central Peruvian coast is weaker, and is a minimum during its high-wind season (June to September).

### 2.4. Coastal upwelling centres

As noted in Section 2.2, the seasonal variation in the three broad areas of high-wind speed in central Perú and central-south Chile (centred at 15, 30, and 37°S, respectively) seems controlled by the intensity of the APG, which in turn is modulated by the annual cycle of the SE Pacific subtropical anticyclone. Embedded in

 

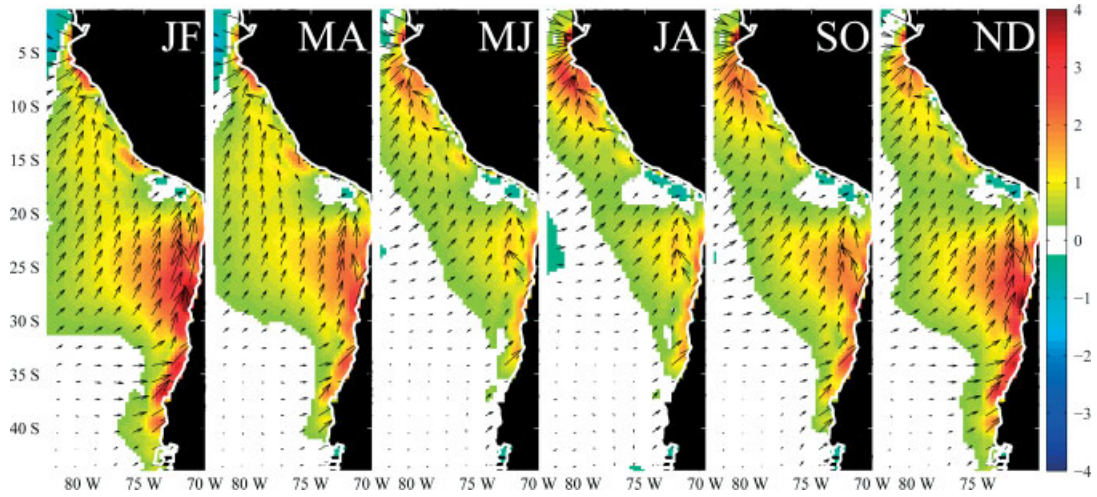


Figure 4. Bimonthly mean (1979–2010) of the 00–12 UTC 10-m wind vector difference and wind speed difference (m $s^{-1}$, colour) from CFSR. Vectors shown at every fifth grid point.

these broad areas, the seasonal mean maps in Figure 2 hint at the existence of smaller wind maxima tied to the coast near Lavapie, LdV, and Pisco. These so-called 'coastal jets' (to differentiate them from the broader low-level jets) have been identified using aircraft data around Lavapie (Montecinos *et al.*, 2011) and LdV (Garreaud *et al.*, 2011) and using *in situ* radiosondes off Pisco (Grados *et al.*, 2010), revealing near-surface wind speed in excess of 20 $ms^{-1}$ in a core of about 40 km long and 20 km wide. The occurrence of these coastal jets fosters very active upwelling in each of these three regions as evidenced by satellite imagery and *in situ* measurements of SST (Sobarzo *et al.*, 2007).

Pisco, LdV, and Lavapie, the three regions in which coastal jets are recurrent, feature a similar geography (Figure 5). South (upstream) of these points the coastline is nearly straight north–south (NW–SE in the case of Pisco). North of these points the coastline retracts inland a few tens of kilometres forming wide, northwest-facing embayments. This suggests mesoscale processes tied to the coastal topography acting in concert with large-scale forcing (the APG) to produce these local coastal jets. For the case of LdV, it was shown that such coastal geometry favours enhanced baroclinicity just north of the point due to the thermal contrast between cool marine air and warm continental air advected from the land over the bay and leads to a local afternoon wind maxima (Garreaud *et al.*, 2011; Rahn *et al.*, 2011).

Hydraulic expansion fan analogues have often been invoked to explain coastal wind maxima elsewhere (Winant *et al.*, 1988; Haack *et al.*, 2001; Dorman and Koracin, 2008). This explanation requires coastal topography acting as a lateral wall that bounds low-level flow within a shallow marine boundary layer (MBL). If the flow is supercritical the MBL collapses in the lee of a convex bend and the wind speed increases. A more or less continuous coastal range exists south of Pisco and LdV, but elevations lower than 300 m exist to the south of Lavapie, subtracting generality to the expansion fan hypothesis for this particular wind maximum, assuming MBL depths over 300 m. In this work, however, we have refrained from diagnosing these coastal jets because the horizontal resolution of CFSR and QuikSCAT (~30 km) is marginal to resolve them.

## 3. Intraseasonal and interannual variability

Associated with the mean migration of the SEP anticyclone are changes in not only the mean but also the distribution of the daily (00 UTC) alongshore wind component at each of the three upwelling centres (Figure 6). The alongshore wind component is calculated similar to Dewitte *et al.* (2011) where the zonal and meridional components were projected onto the mean direction of the coastline that was calculated by a linear regression of the coastal points in ~3° width segments around the centre point. At Pisco, the variation of the alongshore wind is normally distributed with a seasonal shift of the mean and little change in the width (variance) of the distribution. During the summer months at LdV, the distribution is close to a normal distribution as well, but during the other parts of the year it becomes skewed towards weaker wind, especially in the winter months. The skew is attributed to the passage of cyclones that leads to intermittently weaker southerlies and sometimes a reversed (northerly) wind direction. At Lavapie the distribution is skewed toward northerly wind in all seasons, reflecting its closer proximity to the mid-latitude storm track. The distribution becomes nearly uniform in winter, reflecting the frequent passage of weather systems. When the anticyclone strengthens and migrates back south during the summer months, the distribution becomes more normal with a prominent cluster around strong southerly wind, causing the increase in the mean wind.

The long record of CFSR data permits us to describe the interannual variability of the coastal winds in the three major upwelling regions that is represented in Figure 7 by simply averaging the alongshore wind over

 

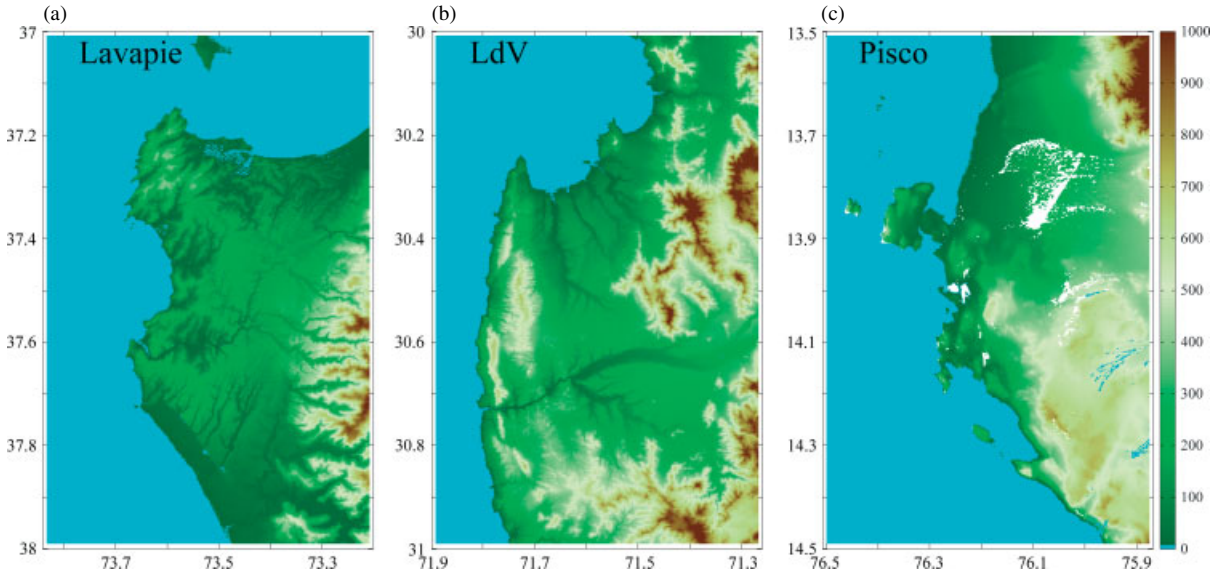


Figure 5. Elevation map (m) from the three arc-second (∼90 m) Shuttle Radar Topography Mission for (a) Lavapie, (b) LdV, and (c) Pisco.

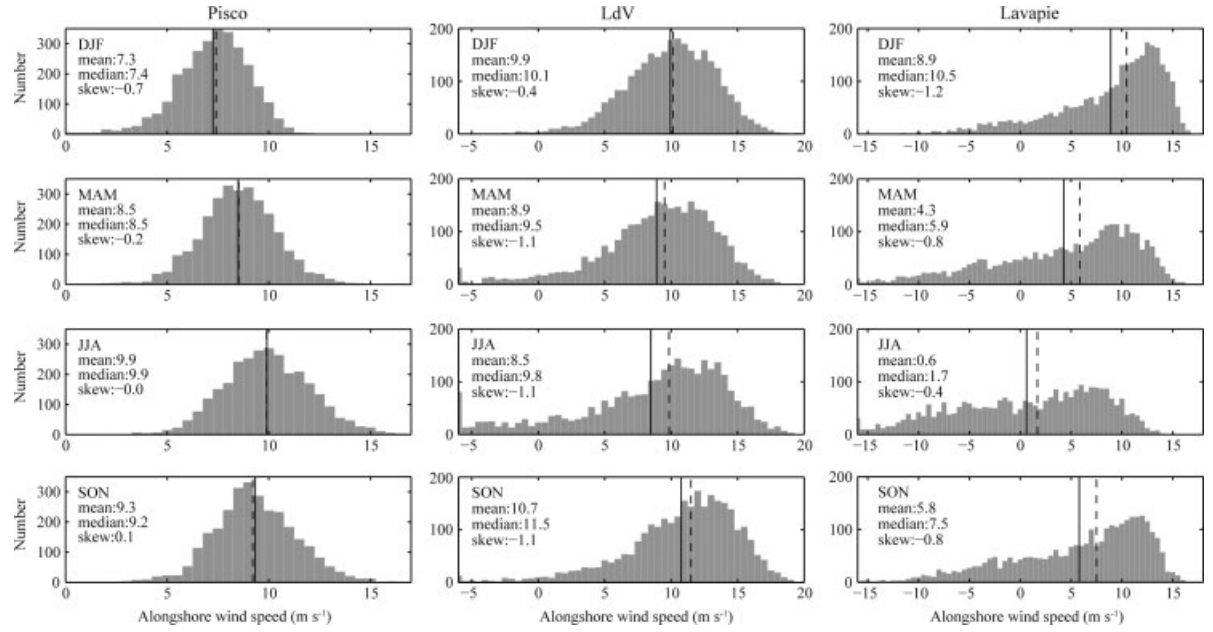


Figure 6. Histogram of the 00 UTC alongshore wind speed (m $s^{-1}$, positive from the south) for Pisco, LdV, and Lavapie. Months are indicated in each panel along with the mean, median and skewness. Vertical lines represent the mean (solid) and median (dashed).

each year. LdV has the most interannual variability with a standard deviation of 0.69 m $s^{-1}$ followed by Lavapie with a standard deviation of 0.57 m $s^{-1}$. Neither appears to have a trend over the last 30 years. Some of the most substantial interannual variations tend to coincide with variation of the El Niño Southern Oscillation (ENSO). When anomalous warm (cold) sea surface temperatures over the Pacific happen during El Niño (La Niña), there is often a decrease (increase) in the mean alongshore wind. The greatest year to year change occurred from 1997 when there was a strong El Niño to 1998 when there was a strong La Niña. The phase of ENSO impacts the atmospheric circulation such that during La Niña the SEP anticyclone is reinforced, leading to a greater APG and more alongshore wind (Rahn, 2012). During El Niño the SEP anticyclone weakens, leading to a smaller APG and less alongshore wind, which is also associated with the more frequent passage of cyclones and greater precipitation in central Chile (30–38°S, Montecinos and Aceituno, 2003). In spite of its lower latitude, Pisco has the least interannual variability (standard deviation of 0.36 m $s^{-1}$), does not seem to be that closely related to ENSO, but does appear to have an upward trend since the alongshore wind has increased about 1 m $s^{-1}$ from 1995 to 2010, which is consistent with earlier findings (Bakun, 1990). On the contrary, using a statistical downscaling of the sea surface wind, Goubanova *et al.* (2010) have suggested a weakening of alongshore wind during austral

 

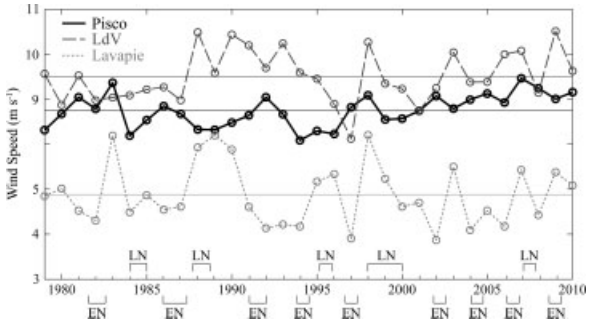


Figure 7. Time series of the mean alongshore wind (m $s^{-1}$) from CFSR at 00 UTC over the entire year at Pisco (solid), LdV (dashed), and Lavapie (dotted) from CFSR. El Niño (EN) and La Niña (LN) are indicated along the bottom axis. Mean of the entire series is indicated by the horizontal line. Note the break in scale of the vertical axis between LdV and Lavapie.

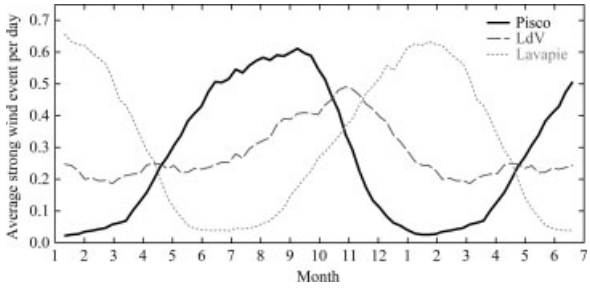


Figure 8. Average number of strong wind events per day at Pisco (solid), LdV (dashed), and Lavapie (dotted) from CFSR at 00 UTC.

winter in warmer climates due to a general decrease in the intraseasonal variability.

## 4. Low-level jet events

### 4.1. Event climatology

Previous studies using *in situ* observations in the three broad areas of high-wind speed have documented short-lived events of strong southerly wind with significant impacts in the upper-ocean circulation (Huyer *et al.*, 1987; Garreaud *et al.*, 2011; Montecinos *et al.*, 2011; Aguirre *et al.*, 2012). The wind speed increases with height throughout the MBL to reach a maximum just below the inversion base, consistent with a thermal wind equilibrium considering sea surface temperature warming offshore and MBL depth increasing offshore. Here, we identify 'windy' days as those belonging to the upper quartile of the full alongshore wind speed distribution. The threshold is 10 m $s^{-1}$ at Pisco, 13 m $s^{-1}$ at LdV, and 11 m $s^{-1}$ at Lavapie. The annual cycle of the strong wind day frequency (Figure 8) is clearly distinct for the three primary upwelling regions and it is similar to the annual cycle of the mean wind and APG in those areas. Spatial features of the windy days are revealed by the average maps in Figure 9. The common feature for high-wind events at each location is a strong anticyclone over the SEP. Subtle synoptic differences that favour high winds in one region over another will be explored later through composites of the synoptic anomalies. An elongated area of strong southerly wind extends around the coastal point for several hundred kilometres. While high-wind events often occur at only one location, about a third of the time when there is a high-wind event at Lavapie or Pisco, there is also a concurrent high-wind event at LdV.

Strong wind days also tend to cluster in short-lived events. This behaviour is illustrated in Figure 10 through a sample time series of the alongshore wind speed for each of the areas of high winds, using a single grid point near the average maximum of the particular low-level jet. Considering the full time series, the mean event duration in days is $2.7 \pm 2.2$ at Pisco, $2.2 \pm 1.6$ at LdV, and $2.6 \pm 2.2$ at Lavapie. Only about 10% of the cases extend more than 4 d at each location. Likewise, the average separation between events is 6–7 d for all three locations. We define a low-level jet event as a sequence of one or more windy days, whose mean features are analysed here using a compositing analysis. The event is defined from 'day 0' that is the first windy day of a sequence. Composites of the conditions 2 d and 1 d before the event are 'day − 2' and 'day − 1', respectively. One day after the start of the event is 'day + 1' and 1 d after the last day of the entire set of sequential days is 'end + 1'. Stricter criteria such as a minimum separation between events and a minimum duration of the event yielded similar results. The composite evolution of the alongshore wind speed for Pisco, LdV, and Lavapie normalized by the mean wind during the event is presented in Figure 11. Consistent with the weak synoptic variability at lower latitudes, the composite evolution at Pisco exhibits the least change in the mean and the smallest standard deviation with the maximum southeast wind during the event slightly larger (~2 m $s^{-1}$) than the wind observed before or after the event. At the other extreme, the onset of a coastal southerly jet event off Lavapie is preceded by a significant increase in wind speed (~6 m $s^{-1}$), and in many cases this includes northerly flow before the strong southerly wind. The wind evolution at LdV exhibits a moderate wind increase from day −1 to day 0, although jet events there are usually preceded by relaxed southerlies rather than weak northerlies.

### 4.2. Synoptic forcing

The episodic character and quasi-weekly recurrence of low-level jet events indicate that they are associated with transient synoptic systems. The typical synoptic environment responsible for the high wind at each site is illustrated in Figure 12 by the composite anomalies of the 10-m wind, SLP, and 500-hPa height. The anomalies are obtained from removing the mean annual cycle that was calculated by first calculating the daily 00 UTC means and then smoothing them in a moving 1 week window. Anomalies are used instead of the full fields because they remove any seasonal or diurnal dependence on the high-wind event that tends to mask the anomalous synoptic conditions. A common ingredient for the occurrence of

 

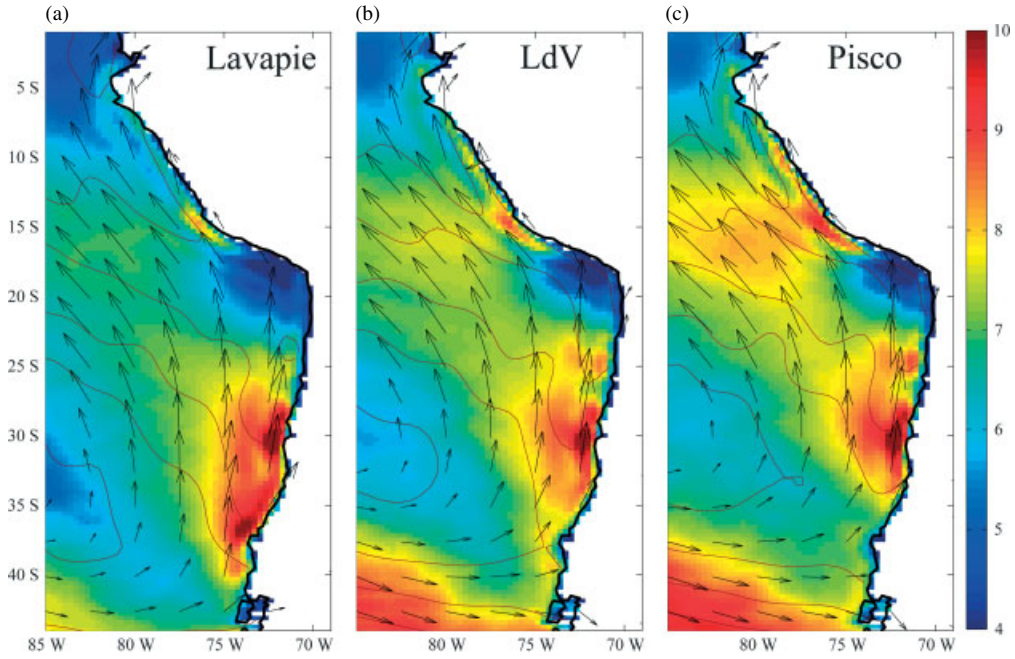


Figure 9. Mean 10-m wind vectors and wind speed (m $s^{-1}$, colour) for the days with an alongshore wind speed in the upper quartile at (a) Lavapie, (b) LdV, and (c) Pisco.

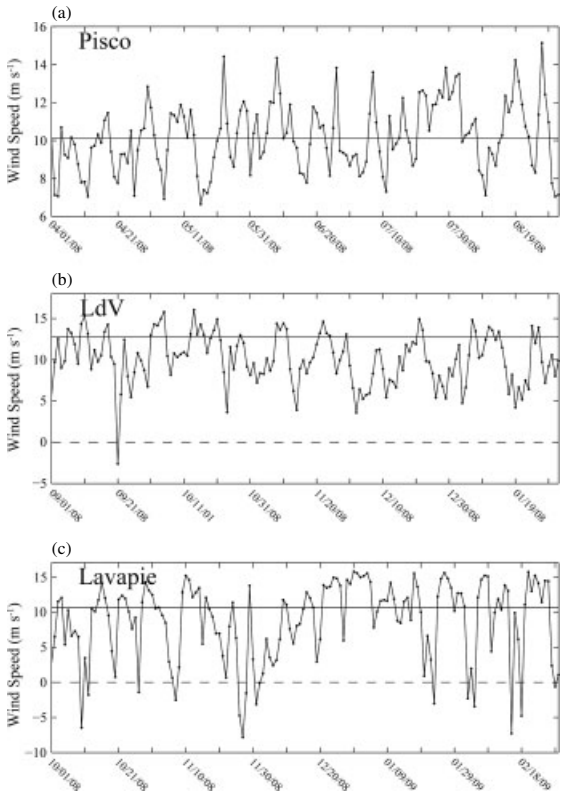


Figure 10. Examples of the time series of alongshore wind speed (m $s^{-1}$) at (a) Pisco, (b) LdV, and (c) Lavapie from CFSR. Vectors shown at every eight grid point.

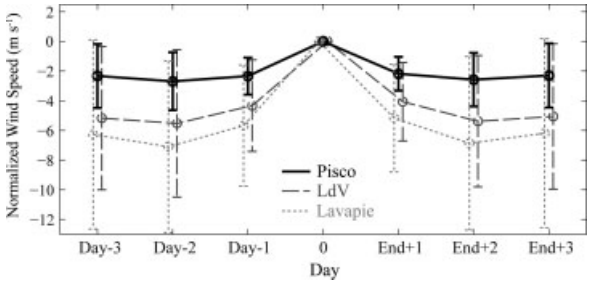


Figure 11. Mean daily evolution of the alongshore wind speed (m $s^{-1}$) using the upper quartile of strong wind days for Pisco (solid), LdV (dashed), and Lavapie (dotted) from CFSR at 00 UTC. Vertical bars indicate the standard deviation.

high wind is the eastward propagation of a baroclinic system at mid- and subtropical latitudes. Two days before the start of the event there is a surface low over the SEP with the trough axis at 500 hPa just west of the surface low centre. In the case of Lavapie the trough and low advance rapidly such that at day 0 they have moved inland and the SEP is under a strong surface anticyclone and mid-level ridge. In the composite for LdV, the system moves slower, but the migratory surface anticyclone has also reached the coast at day 0 under a SW–NE tilted mid-level ridge. In contrast, the surface anticyclone and a SE–NW titled mid-level ridge aloft are still far from the coast at day 0 for the Pisco composite, and the axis of the negative SLP anomaly is off central Chile. Nevertheless, an area of positive SLP anomalies develops in the near-coastal area to the north of 30°S. The origin of this intriguing surface ridging under a mid-level trough is analysed later by mean of a case study, which also demonstrates that the composite reflects the individual members.

Coastal ridging south of the high-wind area is also depicted by the evolution of the average alongshore SLP

 

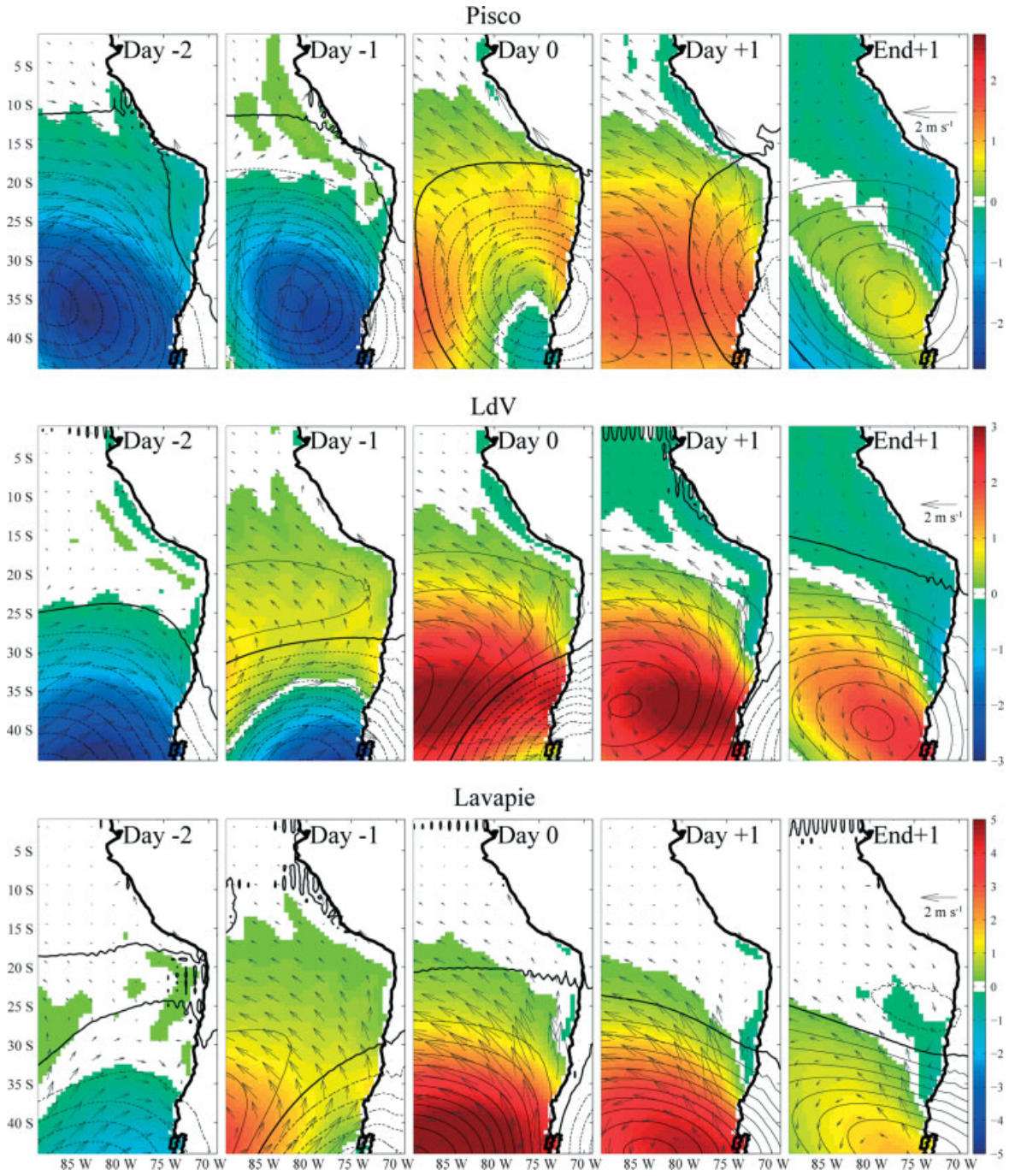


Figure 12. Composites of the 500-hPa height anomalies (5 m, positive contours solid, negative contours dashed, and zero contour bold), SLP anomalies (hPa, colours), and 10-m wind speed anomalies (vectors, m $s^{-1}$) for days relative to event indicated in the upper right of each figure for (top) Pisco, (centre) LdV, and (bottom) Lavapie, from CFSR at 00 UTC. Vectors shown at every fifth grid point.

anomalies (Figure 13). For Pisco there is a broad, extensive positive anomaly peaking at 35°S, while for LdV and Lavapie the anomaly is concentrated over a much shorter distance. In all three cases an enhanced northward APG appears as a necessary condition for the occurrence of a high-wind day, extending early findings for the LdV sector (Muñoz and Garreaud, 2005) where the relationship $v_{sfc} \sim$ APG was attributed to the geostrophic breakdown by the coastal topography. Note that in the case of Pisco a relatively weak, positive APG is capable of producing a strong wind day, consistent with a relatively weak change in APG in Figure 3 that is able to drive the seasonal variations. On the other hand, a strong APG at day 0 occurs along a vast portion of the coast but the area of highest wind is much more confined around the coastal points (Pisco, LdV, or Lavapie) indicative of a mesoscale control of the low-level flow (Rahn *et al.*, 2011).

Returning to the composite maps in Figure 12, we note some common ingredients the day after the demise of the jet events (end + 1). In all three cases, the surface

 

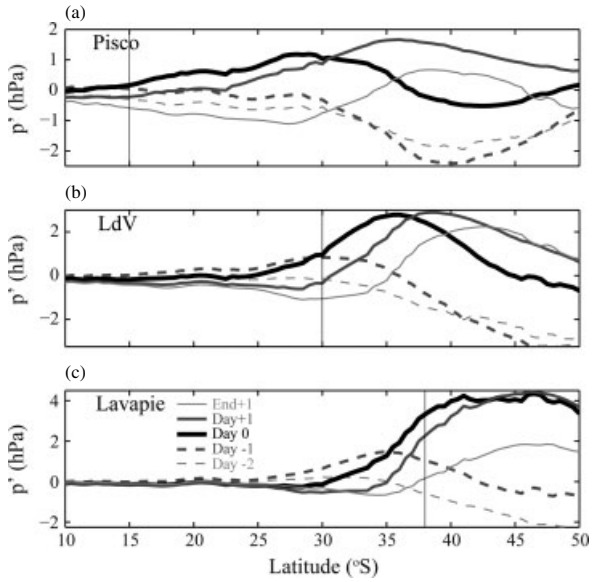


Figure 13. Alongshore SLP perturbation (hPa) at 00 UTC associated with strong wind events at (a) Pisco, (b) LdV, and (c) Lavapie. Day relative to the event is indicated by the key in (c). Location of each upwelling centre is indicated by a vertical line.

anticyclone has weakened and its centre is just off the coast directly underneath a mid-level ridge. At the same time, negative pressure anomalies develop along the coast of north-central Chile, decreasing or even reversing the APG in that region (Figure 13). While in Pisco and LdV the negative SLP anomalies are not associated with northerly wind anomalies, a day after the wind event at Lavapie there are northerly wind anomalies along much of the coast. The coastal troughing after the peak of the coastal wind has been previously reported in central Chile (Garreaud *et al.*, 2002; Garreaud and Rutllant, 2003).

### 4.3. Case study

Coastal ridging before a jet event off LdV and Lavapie is largely explained by the anticyclonic vorticity advection in the middle troposphere in connection with the incoming ridge aloft. This is not the case for Pisco, where the ridging occurs under cyclonic vorticity advection. To help explain this synoptic pattern, an example of the synoptic conditions for a particular high wind event on 17 September 1986 is shown in Figure 14. This case is representative of the typical conditions associated with high-wind events at Pisco. As the negatively tilted trough approaches the central Chilean coastline, a local low pressure perturbation at the surface develops cyclonic rotation 1 d prior to the event. North of the centre of rotation there is an onshore wind component and a tongue of higher SLP that extends towards the coast, similar to the day 0 composite in Figure 12. The onshore wind under an eastward propagating trough results in a large impact on the lower atmosphere and the MBL in particular. Figure 15 depicts a series of cross-sections along 25°S during this event. As the trough moves toward the coast, the MBL expands into a fairly deep mixed layer (~2 km or 800 hPa at 76°W) on 16 September, corresponding to the enhanced onshore wind and higher SLP seen in the surface chart. The trough relaxes over the next couple days and the MBL thins to its more normal depth (~1 km or 900 hPa), which is also associated with a diminishing surface pressure anomaly.

Deepening of the MBL and the corresponding increase of SLP over the SEP prior to the high-wind event at Pisco is driven by two major processes: low-level convergence and cold air advection (Figure 16). Temperature advection is calculated as an average in the 900–700 hPa layer to better represent the lowest levels and remove some of the noise inherent in the field. Two days prior to

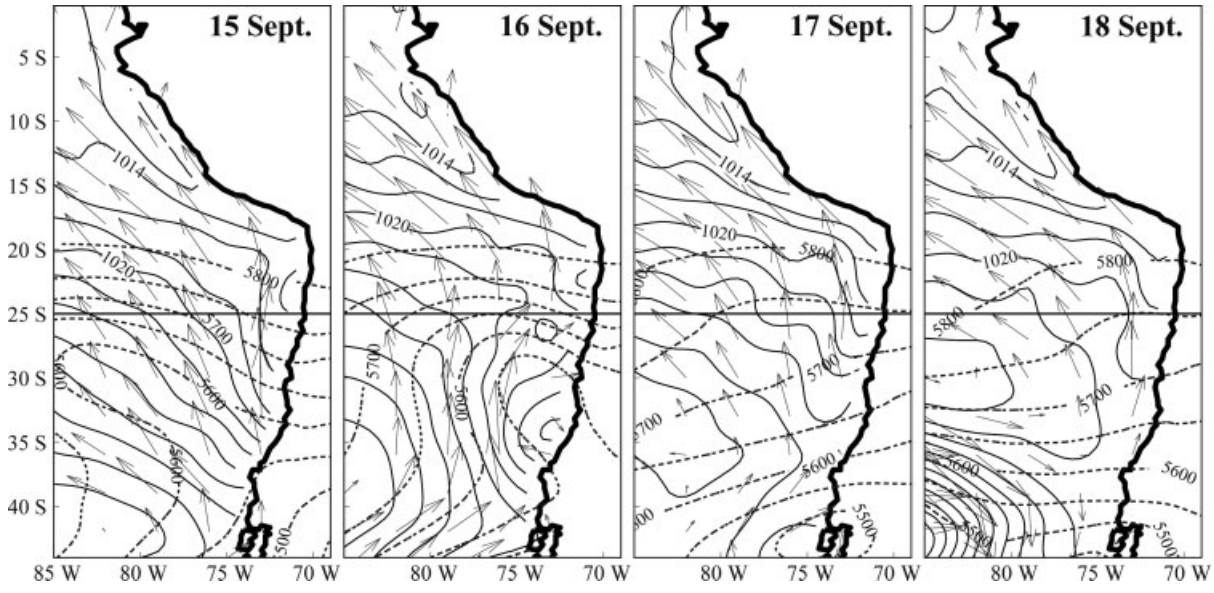


Figure 14. Surface pressure (hPa, solid), 500 hPa height (m, dashed), and 10-m wind vectors from the CFSR at 00 UTC. Horizontal line indicates location of cross-section in Figure 15. Vectors shown at every eight grid point.

 

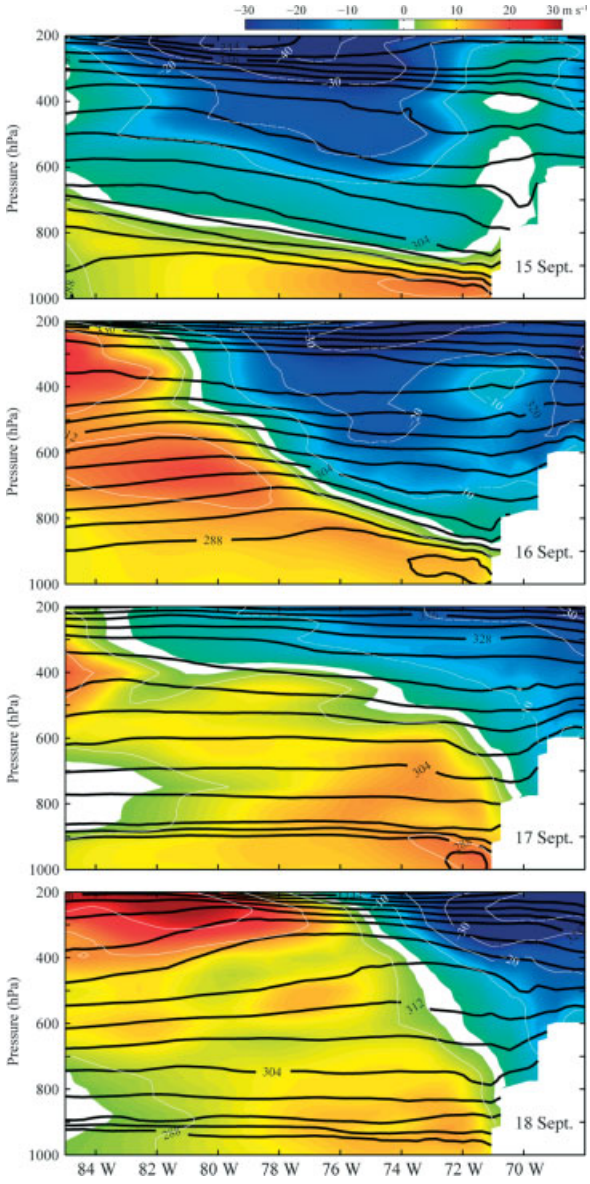


Figure 15. Vertical cross-section at 00 UTC along 25°S showing meridional wind speed (m $s^{-1}$, colour) and potential temperature ($K$, black contours).

the start of the high-wind event there is cold air advection over much of the region and it reverses to warm air advection on the day of the event. The result is a marked cooling in this layer (Figure 15(b)). Concurrently, in the 1000–900 hPa layer, there is convergence between the coast and 75°W that is forced by the interaction of the cyclonic circulation near the coast in central Chile and the steep topography in northern Chile that blocks the onshore flow. The MBL must respond to the mass convergence by becoming deeper. A cooler lower atmosphere and a deeper MBL contribute to higher SLP, especially concentrated along the coast. The greater SLP anomaly in northern Chile leads to stronger forcing of surface winds to the north and at Pisco. On day + 1 when the wind is strong around Pisco, there is a marked dipole of divergence around the wind maximum.

## 5. Summary

Intermittent and sparse *in situ* meteorological measurements have impeded a general climatology along the west coast of South America, especially true offshore given the small number of buoy data. With the advent of satellite scatterometer observations, our understanding has advanced considerably, but these measurements have their own limitations and do not provide information on other key atmospheric variables such as surface pressure. To overcome these issues, we employed the CFSR, a high-resolution reanalysis (grid spacing 0.313°) that synthesizes as much observational data into a physically consistent, best estimate of the real state of the atmosphere. Older reanalyses with a grid spacing of 2.5° lacked sufficient horizontal resolution to adequately represent local low-level jets associated with mesoscale interactions with prominent points along the coast. Indeed, specific attention here is placed on three points known for their enhanced upwelling: Pisco, LdV, and Lavapie. Each location exhibits a marked seasonal cycle of strong wind days, which result from a shift in the mean wind and more frequent reoccurrence of strong wind events. The synoptic evolution that drives high-wind events at each location is generalized and contrasted.

Furthermore, covariability between the APG and alongshore wind, which was previously identified for synoptic time scales near central Chile, is generalized for the whole coast and over annual time scales. These results may be used as a baseline for any future changes to the atmospheric circulation in the region. Some specific highlights are listed below.

- Interannual variation of the alongshore wind is smallest at Pisco, where the alongshore wind speed has been increasing since 1995. Interannual variation is greatest at Lavapie and LdV, where there is also influence from ENSO.
- Maximum mean wind peaks during September at Pisco, during November at LdV, and during January at Lavapie. Pisco and Lavapie have a large annual cycle in the likelihood of high-wind events that are out of phase with each other. High-wind events at LdV are more evenly distributed throughout the year.
- A normal distribution describes the alongshore wind year-round at Pisco and during the spring and summer at LdV. A tail towards northerly wind becomes more prominent in the winter months due to the increase of winter synoptic activity, but the distribution always contains a cluster for strong southerly wind, except at Lavapie during winter when the distribution becomes nearly uniform.
- Synoptic conditions during a high-wind event at Lavapie are preceded by a midlevel trough and surface cyclone that move quickly eastward. Midlevel ridging and an enhancement of the surface cyclone under anticyclonic vorticity advection are present at the start of the event. Synoptic conditions during a high-wind event at LdV are similar to Lavapie but the midlevel trough and surface cyclone move eastward somewhat

 

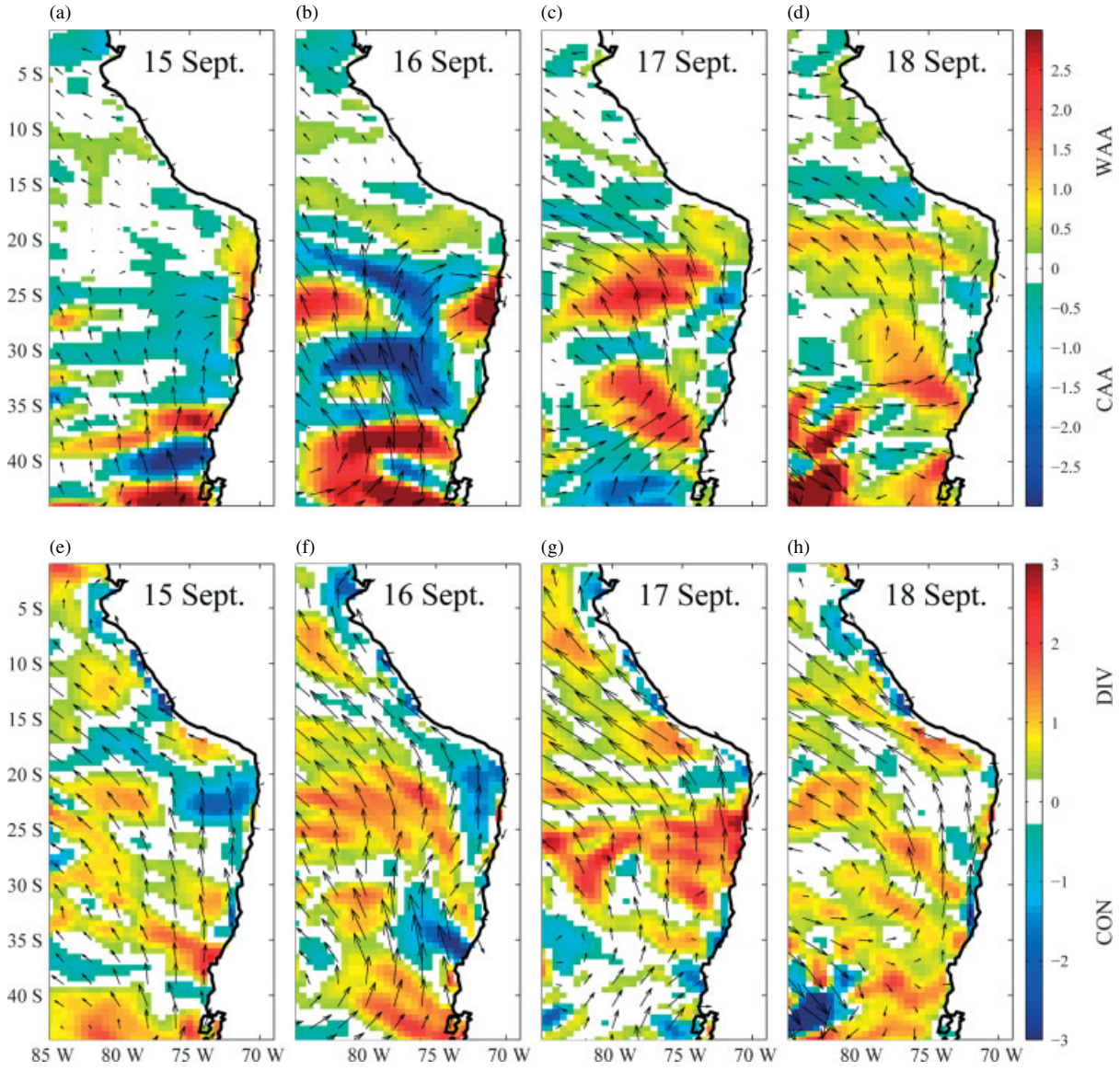


Figure 16. From CFSR at 00 UTC. (a–d) Average temperature advection ($10^{-4}$ C $s^{-1}$) and wind vectors (m $s^{-1}$) in the 700–900 hPa layer. (e–f) Average divergence ($10^{-5}$ $s^{-1}$) and wind vectors (m $s^{-1}$) in the 900–1000 hPa layer. Vectors shown at every fifth grid point.

slower. The midlevel trough is on average positively tilted and the low-level wind reaches a maximum just after the surface cyclone and trough pass the Andes Cordillera.

- Synoptic conditions during a high-wind event at Pisco are typified by a negatively tilted midlevel trough propagating slowly eastward and the wind speed reaches a maximum when the trough is still over the Pacific. Despite being ahead of an easterly propagating trough where one would expect anomalously low SLP, a combination of cold air advection and surface convergence in northern Chile/southern Peru leads to an anomalously cool lower atmosphere and a deep MBL, leading to a high SLP anomaly south of Pisco, and a stronger pressure gradient force that drives the high-wind event.
- After the end of the strong wind event at all three locations, negative SLP anomalies are found along north-central Chile. Northerly wind anomalies are also present 1 d after the strong wind event at Lavapie.

## Acknowledgements

DAR was supported by FONDECYT 3110100 and New Faculty Startup funds at KU and RDG was supported by FONDAP CR2 (Grant 15110009).

## References

Aguirre C, Pizarro O, Strub T, Garreaud R, Barth J. 2012. Seasonal dynamics of the alongshore flow off central Chile. *Journal of Geophysical Research* **116**: C01006. DOI: 10.1029/2011JC007379.

Bakun A. 1990. Global climate change and intensification of coastal ocean upwelling. *Science* **247**: 198–201.

Brink KH, Allen JS, Smith RL. 1978. A study of low-frequency fluctuations near the Peru Coast. *Journal of Physical Oceanography* **8**: 1025–1041.

 

Capet X, Colas F, McWilliams JC, Penven P, Marchesiello P. 2008. Eddies in eastern boundary subtropical upwelling systems, in Ocean Modeling in an Eddying Regime. *Geophysical Monograph Series – AGU* **177**: 131–148.

Dee DP, Uppala SM, Simmons AJ, Berrisford P, Poli P, Kobayashi S, Andrae U, Balmaseda MA, Balsamo G, Bauer P, Bechtold P, Beljaars ACM, van de Berg L, Bidlot J, Bormann N, Delsol C, Dragani R, Fuentes M, Geer AJ, Haimberger L, Healy SB, Hersbach H, Háolm EV, Isaksen L, Kăllberg P, Köhler M, Matricardi M, McNally AP, Monge-Sanz BM, Morcrette J-J, Park B-K, Peubey C, de Rosnay P, Tavolato C, Thépaut J-N, Vitart F. 2011. The ERA-Interim reanalysis: configuration and performance of the data assimilation system. *Quarterly Journal of the Royal Meteorological Society* **137**: 553–597. DOI: 10.1002/qj.828.

Dewitte B, Illig S, Renault L, Goubanova K, Takahashi K, Gushchina D, Mosquera K, Purca S. 2011. Modes of covariability between sea surface temperature and wind stress intraseasonal anomalies along the coast of Peru from satellite observations (2000–2008). *Journal of Geophysical Research* **116**: C04028. DOI: 10.1029/2010JC006495.

Dorman CE, Koracin D. 2008. Response of the summer marine layer flow to an extreme California coastal bend. *Monthly Weather Review* **136**: 2894–2992.

Escribano R, Rosales SA, Blanco JL. 2004. Understanding upwelling circulation off Antofagasta (northern Chile): a three-dimensional numerical-modeling approach. *Continental Shelf Research* **24**: 37–53.

Garreaud RD, Muñoz RC. 2005. The low-level jet off the West Coast of subtropical South America: structure and variability. *Monthly Weather Review* **133**: 2246–2261.

Garreaud RD, Rutllant J. 2003. Coastal lows along the subtropical west coast of South America: numerical simulation of a typical case. *Monthly Weather Review* **131**: 891–908.

Garreaud R, Rutllant J, Fuenzalida H. 2002. Coastal lows in north-central Chile: mean structure and evolution. *Monthly Weather Review* **130**: 75–88.

Garreaud RD, Rutllant JA, Muñoz RC, Rahn DA, Ramos M, Figueroa D. 2011. VOCALS-CUpEx: the Chilean upwelling experiment. *Atmospheric Chemistry and Physics* **11**: 2015–2029.

Goubanova K, Echevin V, Dewitte B, Codorn F, Takahashi K, Terray P, Vrac M. 2010. Statistical downscaling of sea-surface wind over the Peru-Chile upwelling region: diagnosing the impact of climate change from the IPSL-CM4 model. *Climate Dynamics*. **36**: 1365–1378 DOI: 10.1007/s00382-010-0824.

Grados C, Chaigneau A, Takahashi K, Dewitte B, Garreaud R, Gallardo L. 2010. VOCALS-REx coastal component. *CLIVAR-Exchanges Newsletter* **15**: 23–28.

Haack T, Burk SD, Dorman C, Rodgers D. 2001. Supercritical flow interaction within the Cape Blanco–Cape Mendocino orographic complex. *Monthly Weather Review* **129**: 688–708.

Halpern D, Woiceshyn P, Zlotnicki V, Brown O, Freilich M, Wentz F 2002. An atlas of monthly mean distributions of SSMI wind speed, AVHRR sea surface temperature, TMI sea surface temperature, QuikSCAT ocean vector wind, SeaWiFS Chlorophill-a, and TOPEX/POSEIDON sea surface topography during 2001. *JPL Publication* 02–23, NASA.

Hill AE, Hickey BM, Shillington FA, Strub PT, Brink KH, Barton ED, Thomas AC. 1998. Eastern ocean boundaries. *The Global Coastal Ocean*: *Regional Studies and Syntheses*, *The Sea* 11 (AR Robinson and KH Brink): John Wiley and Sons, New York, 29–68.

Huyer A, Smith RL, Paluszkiewicz T. 1987. Coastal upwelling off Peru during normal and El Niño times, 1981–1984. *Journal of Geophysical Research* **92**(C1314): 14297–14307.

Kalnay E et al. 1996. The NCEP/NCAR 40-year reanalysis Project. *Bulletin of the American Meteorological Society* **77**: 437–470.

Lindberg C, Broccoli AJ. 1996. Representation of topography in spectral climate models and its effect on simulated precipitation. *Journal of Climate* **9**: 2641–2659.

Montecinos A, Aceituno P. 2003. Seasonality of the ENSO-related rainfall variability in central Chile and associated circulation anomalies. *Journal of Climate* **16**: 281–296. DOI: 10.1175/1520-0442(2003)016<0281:SOTERR>2.0.CO;2.

Montecinos A, Muñoz R, Garreaud R, Arriagada A, Conejero C, Morales J, Burger F, Sánchez E, Vizcarra A. 2011. Experimiento de Surgencia Costera en el Golfo de Arauco (CUPEX-II). *Segundo Congreso de Oceanografta Ftsica, Meteorologta y Clima* Coquimbo, Chile.

Muñoz RC. 2008. Diurnal cycle of surface winds over the subtropical southeast Pacific. *Journal of Geophysical Research* **113**: D13107. DOI: 10.1029/2008JD009957.

Muñoz RC, Garreaud RD. 2005. Dynamics of the low-level jet off the west coast of subtropical South America. *Monthly Weather Review* **133**: 3661–3677.

Rahn DA. 2012. Influence of large scale oscillations on upwelling-favorable coastal wind off central Chile. *Journal of Geophysical Research*, **117**: D19114. DOI:10.1029/2012JD018016.

Rahn DA, Garreaud R, Rutllant J. 2011. The low-level atmospheric circulation near Tongoy Bay / point Lengua de Vaca (Chilean coast 30°S). *Monthly Weather Review* **139**: 3628–3647.

Rodwell MJ, Hoskins BJ. 2001. Subtropical anticyclones and summer monsoons. *Journal of Climate* **14**: 3192–3211.

Saha S *et al.* 2010. The NCEP climate forecast system reanalysis. *Bulletin of the American Meteorological Society* **91**: 1015–1057.

Seluchi ME, Saulo AC, Nicolini M, Satyamurty P. 2003. The north-western Argentinean low: a study of two typical events. *Monthly Weather Review* **131**: 2361–2378.

Sherman K, Hempel G (eds). 2009. *The UNEP Large Marine Ecosystem Report: a perspective on changing conditions in LMEs of the world's Regional Seas. UNEP Regional Seas Report and Studies* No. 182. United Nations Environment Programme Nairobi: Kenya.

Sobarzo M, Bravo L, Donoso D, Garcés-Vargas J, Schneider W. 2007. Coastal upwelling and seasonal cycles that influence the water column over the continental shelf off central Chile. *Progress in Oceanography* **75**: 363–382.

Wang Y, Xie SP, Want B, Xu H. 2005. Large-scale forcing by southeast Pacific boundary layer clouds: a regional model study. *Journal of Climate* **18**: 934–951.

Winant CD, Dorman CE, Friehe CA, Beardsley RC. 1988. The marine layer off northern California: an example of supercritical channel flow. *Journal of Atmospheric Science* **45**: 3588–3605.

Woodruff SD, Worley SJ, Lubker SJ, Ji Z, Freeman JE, Berry DI, Brohan P, Kent EC, Reynolds RW, Smith SR, Wilkinson C. 2011. ICOADS Release 2.5: extensions and enhancements to the surface marine meteorological archive. *International Journal of Climatology* **31**: 951–967.

 